RESEARCH ARTICLE

Optimization of pore structure and wet tribological properties of paper-based friction materials using chemical foaming technology

Chang LI, Jie FEI[*]**, Enzhi ZHOU, Rui LU, Xiaohang CAI, Yewei FU, Hejun LI**

State Key Laboratory of Solidification Processing, Shaanxi Province Key Laboratory of Fiber Reinforced Light Composite Materials, Northwestern Polytechnical University, Xi'an 710072, China

© The author(s) 2021.

Abstract: Paper-based friction materials are porous materials that exhibit anisotropy; they exhibit random pore sizes and quantities during their preparation, thereby rendering the control of their pore structure difficult. Composites with different pore structures are obtained by introducing chemical foaming technology during their preparation to regulate their pore structure and investigate the effect of pore structure on the properties of paper-based friction materials. The results indicate that the skeleton density, total pore area, average pore diameter, and porosity of the materials increase after chemical foaming treatment, showing a more open pore structure. The addition of an organic chemical foaming agent improves the curing degree of the matrix significantly. Consequently, the thermal stability of the materials improves significantly, and the hardness and elastic modulus of the matrix increase by 73.7% and 49.4%, respectively. The dynamic friction coefficient increases and the wear rate is reduced considerably after optimizing the pore structure. The wear rate, in particular, decreases by 47.7% from 2.83×10^{-8} to 1.48×10^{-8} cm^3/J as the foaming agent content increases. Most importantly, this study provides an effective method to regulate the pore structure of wet friction materials, which is conducive to achieving the desired tribological properties.

Keywords: paper-based friction materials; chemical foaming technology; pore structure; tribological properties

1 Introduction

Paper-based friction materials are typically synthesized via wet paper-making methods, using reinforced fibers and friction modifiers as the main raw materials to create preforms, which are then impregnated with binders and cured via hot pressing [1–4]. As a type of composite, paper-based friction materials can exhibit excellent performance not afforded by a single component through performance coupling among different components, e.g., a high and stable dynamic friction coefficient (μ_d), high torque transmission ability, low friction noise, and high wear resistance [5]. Paper-based friction materials are porous materials.

During material preparation, the random arrangement and bridging of fibers, the air entrainment of each component, and the escape of low-molecular gas products generated in the resin curing reaction can create pores inside the materials, which renders it difficult to control the pore structure. However, it is often indicated that the pore structure is an important factor that affects the thermal, mechanical, and tribological properties of wet friction materials [6–11]. Therefore, the pore structure must be regulated and optimized to improve the comprehensive performance of paper-based friction materials.

In previous studies, the porosity was modified and its effect on the tribological properties of paper-based

---

* Corresponding author: Jie FEI, E-mail: feijiecc@nwpu.edu.cn

composites was analyzed. Deng et al. [6] prepared several paper-based friction materials with different porosities by changing the thickness of the material. The results indicated that as the porosity increased, μ_d and compressibility increased, whereas the recovery rate decreased. Matsumoto [12] varied the porosity of paper-based friction materials by changing the fibrillation degree of the fibers. The experimental results indicated that the maximum temperature of the friction surface during the engagement process decreased when the porosity of the material was higher. Ren et al. [13] discovered that the porosity of the materials decreased gradually as the curing pressure increased. Zhu et al. [14] concluded that wear rate increased with an increase in porosity, and the wear resistance of high-porosity materials decreased owing to their loose and porous structure. Current investigation into the pore structure of paper-based friction materials indicates two deficiencies. First, the pore structure control of the material is performed based on a single method, i.e., primarily by changing the material thickness or hot-pressing curing parameters. Second, existing studies show that an increase in porosity increases the wear rate, which hinders the simultaneous improvement in friction and wear performance. Therefore, an effective method is necessitated to regulate the pore structure of paper-based friction materials such that the materials can yield a higher μ_d while maintaining a low wear rate.

Chemical foaming is a process in which a chemical foaming agent decomposes thermally and releases gas during processing to foam the material; this is primarily used for the foaming of concrete, sponge, and thermoplastics [15–19]. A chemical blowing agent is characterized by its thermal decomposition within a specific temperature range and can release one or more gases, thereby rendering it suitable for polymers that exhibit the molten state within a specific temperature range [20]. Organic chemical foaming agents offer the advantages of constant decomposition temperature, significant gas production, and good dispersion in polymers. The gas produced by the thermal decomposition of an organic chemical foaming agent is primarily nitrogen, which exhibits the lowest permeability to polymer and cannot easily escape from the foam body quickly. Therefore, nitrogen, as

the most effective foaming gas, significantly improves foaming efficiency [21]. Paper-based friction materials with different pore structures can be obtained by changing the amount of foaming agent. However, few studies have applied chemical foaming technology to regulate the pore structure and investigate its effect on the overall properties of paper-based friction materials.

In this study, paper-based friction materials with different pore structures were achieved by introducing chemical foaming technology during their preparation. The decomposition characteristics and activation mechanisms of the foaming system were analyzed. The pore structures of different materials were characterized, and their thermal, mechanical, and wet tribological properties were compared. In addition, the strengthening effect of the chemical foaming system on the matrix, and the impact mechanism of the pore structure on the tribological performance were investigated.

2 Experimental

2.1 Raw material

The fiber reinforcements included polyacrylonitrile-based carbon fibers (Jilin Jiyan High Technology Fiber Co., Ltd., China), aramid fibers (DuPont, USA), and cellulose fibers, which constituted 33.3%, 31.0%, and 35.7% of the reinforcing fibers, respectively. The mixed fillers were composed of alumina, chromite, mineral, zinc oxide, barium sulfate, talcum, graphite, and carbon black powders, which constituted 20.0%, 20.0%, 15.0%, 15.0%, 12.8%, 7.8%, 5.5%, and 3.9% of the fillers, respectively. The binder comprised equal amounts of a 20 wt% cashew-modified phenolic resin solution (Shandong Shengquan New Material Co., Ltd., China) and a 20 wt% nitrile rubber solution (Hengshui Ruien Rubber & Plastic Technology Co., Ltd., China). N,N'-dinitroso pentamethylene tetramine (DPT, Zhejiang Shuntai Rubber & Plastic Technology Co., Ltd., China) was selected as the organic chemical foaming agent. Urea (Sinopharm Chemical Reagent Co., Ltd., China) was used as the foaming auxiliary for the foaming system to reduce the decomposition temperature.

2.2 Material preparation

Figure 1 shows a diagram of the manufacturing process of the paper-based friction materials, where chemical foaming technology was introduced. First, reinforced fibers, cellulose fibers, fillers, and DPT were mixed with a certain amount of water and stirred for 15 min to form a uniformly dispersed slurry. Subsequently, the slurry was poured into a vacuum suction filter to manufacture the wet preform of the paper-based friction material. Next, the prepared wet preform was placed in an oven and dried at 70 °C for 60 min. Subsequently, the dried preform was immersed in a urea solution and dried at room temperature after the immersion was completed. Next, the dried preform obtained in the second step was immersed in the binder solution and dried at room temperature again after a full immersion. Finally, the dried preform was placed into the curing machine for hot pressing and foam modeling. The foaming time was 10 min, the hot-pressing foaming temperature was 160 °C, and the pressure was 5 MPa. After the hot-pressing foaming was completed, a ring-shaped (outer diameter: 103 mm; inner diameter: 72 mm) paper-based friction material with a thickness of 0.75 mm was obtained by performing a blanking procedure. The relative amounts of the ingredients in the composites are shown in Table 1. The foaming system contained an organic chemical foaming agent and a foaming auxiliary at a weight ratio of 4.3:3.7.

2.3 Testing equipment and method

The friction surfaces of the materials before and after the tribology test were observed using the scanning electron microscope (SEM, Czech Tescan VEGA3, Czech Republic). The surface roughness and three-dimensional (3D) surface profiles before wear were measured using an OPTELICS C130 real color confocal microscope (LASERTEC, Japan).

Fourier transform infrared spectroscopy was used to analyze the chemical groups of the foaming system and to measure the change in the chemical groups of the materials before and after hot-press chemical foaming.

The thermogravimetric and differential scanning calorimetry (TG-DSC) of the DPT and foaming system and the thermal properties of the composites were tested using a thermal gravimetric analyzer (TGA/SDTA851, METTLER TOLEDO, Switzerland). The measurement was performed in the temperature range of 50–800 °C at a heating rate of 10 °C/min and a flow rate of 50 mL/min under an argon atmosphere.

A mercury porosimeter (AutoPore IV 9500, USA) under high pressure was used to characterize the mercury injection curve, skeletal density, average pore
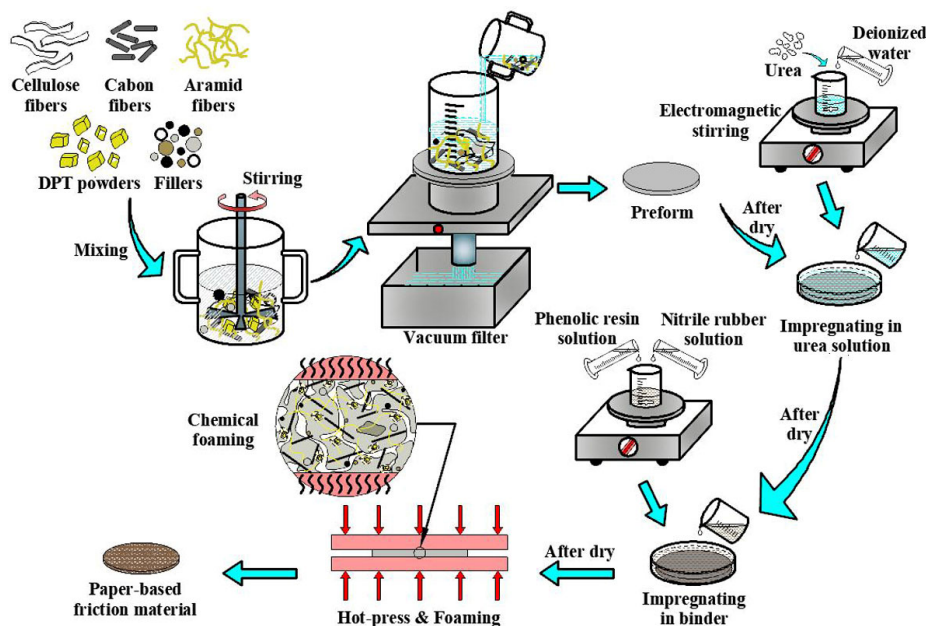

Fig. 1 Diagram illustrating preparation process of paper-based friction materials using chemical foaming technology.

Table 1 Compositions and ratio (wt%) of the samples.

Sample	F1	F2	F3	F4
Fibers	35	35	35	35
Binder	35	35	35	35
Fillers	30	25	20	15
Foaming system	0	5	10	15

diameter, and porosity of the composites. The test range for the pore diameter was 0.003–1,000 μm.

The oil wettability of the samples was tested using a contact angle meter (JC2000D, China), where the liquid medium was the lubricating oil used in the tribology test.

A nanoindentation test (Nano Indenter G200, Agilent Technologies, USA) was used to evaluate the hardness and Young's modulus of the binder matrix under a load of 100 mN. The selected nanoindenter was a Berkovich indenter with a radius of 20 nm.

Compressibility and recovery tests were performed on the paper-based friction materials using a CMT5304-30 KN electronic universal testing machine (Shenzhen SANS Testing Machine Co., Ltd., China) at room temperature. The sample was cut into 10 mm × 10 mm pieces and an initial load of 5 N was applied and maintained for 10 s initially. Subsequently, the sample was loaded uniformly at a speed of 0.2 mm/min until the main load reached 50 N, which was then maintained for 10 s. Finally, it was uniformly unloaded at a speed of 0.2 mm/min until a preload of 5 N was reached. This loading and unloading process of one sample was repeated for three cycles, and the average of the three experimental data was applied for further analysis.

Based on the the standard "GB13826-2008 Wet-type (non-metallic) friction materials", China, the wet tribology properties were characterized using a QM1000-II friction tester (Xi'an Shuntong Science & Technology Co., Ltd., China) under continuous oil-lubricated conditions. The dynamic friction coefficient obtained from each braking was recorded using a testing machine. The wear rate of the materials was calculated after 500 continuous braking cycles under a contact pressure of 0.5 MPa and a rotational speed of 2,000 rpm. The wear rate was calculated as in Eq. (1) [22, 23]:

$$W = \frac{A \times \Delta h}{n \times \frac{1}{2} I_0 \omega^2} \tag{1}$$

where W is the wear rate (cm³/J), A is the apparent contact area of the samples (cm²), Δh is the thickness change of the samples (cm), n is the number of braking cycles, I_0 is the total inertia of the tester (kg·m²), and ω is the angular velocity of the tester (rad/s).

3 Results and discussion

3.1 Characteristics of foaming system

As an organic chemical foaming agent, DPT offers the advantages of easy dispersion, high gas production, and high foaming efficiency [24–26]. As shown in Fig. 2(a), the DPT powder as a block measuring approximately 20 μm. The infrared spectra of DPT and urea were measured using the KBr compression method, and the infrared spectra of DPT and urea are shown in Figs. 2(b) and 2(c), respectively. The characteristic absorption of DPT corresponded to the stretching vibration absorption peak of N=O at 1,265 cm⁻¹, whereas the characteristic absorption of urea corresponded to the bending vibration absorption peak of H–N–H at 1,622 cm⁻¹.

To investigate the decomposition characteristics of the foaming system, TG-DSC analysis was performed on DPT and a mixture comprising DPT and urea. Figures 2(d) and 2(e) show the TG-DSC curves of DPT and the mixture comprising DPT and urea, respectively. As shown in Fig. 2(d), the decomposition of DPT was abrupt. It began to decompose slowly at 170 °C and then decomposed rapidly at 207 °C, with a decomposition peak temperature of 211 °C. At the endpoint of the exothermic peak (220 °C), the weight loss rate of DPT was approximately 83%. The decomposition reaction of DPT is shown in Fig. 3(a). DPT decomposed into nitrogen, formaldehyde, and hexamethylene tetramine (HMTA) after heating [24]. HMTA is the most typically used curing agent for phenolic resins; therefore, the use of DPT as a foaming agent does not introduce additional harmful products after decomposition. However, the decomposition temperature of DPT is relatively high. To match the decomposition temperature of DPT with the curing
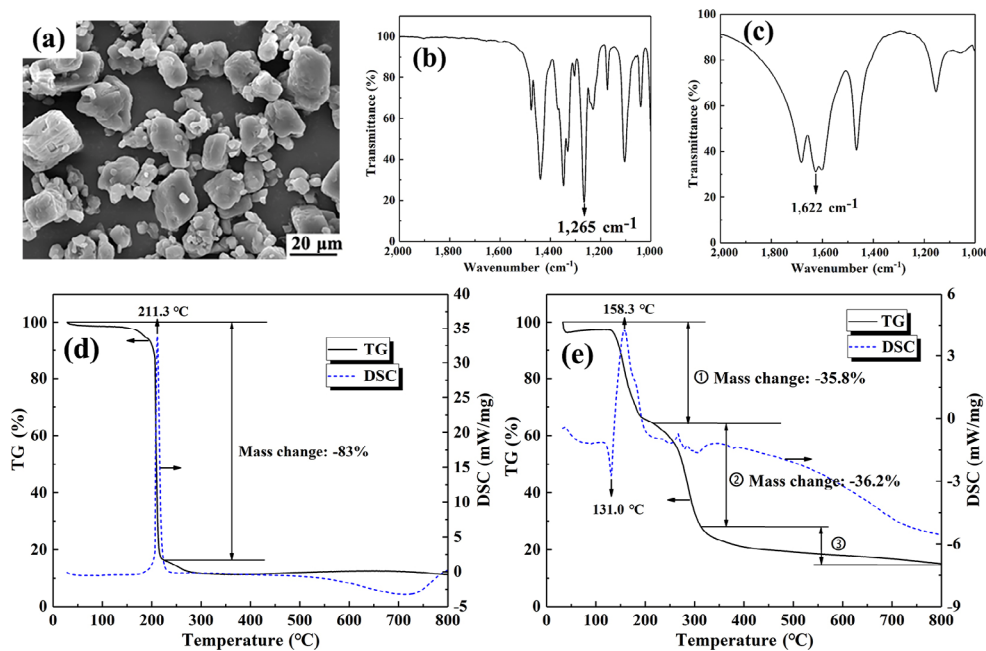
Fig. 2 (a) Micromorphology of DPT; Fourier transform infrared spectroscopy of (b) DPT and (c) urea; (d) TG-DSC curves of DPT and (e) mixture of DPT and urea.

temperature of the binder, urea was added to reduce the decomposition temperature of DPT; this can improve the foaming efficiency and eliminate the peculiar smell generated by the decomposition residue of DPT. As shown in Fig. 2(e), the decomposition process of the combination of DPT and urea differed significantly from that of DPT, and the addition of urea reduced the decomposition temperature of DPT considerably. The reaction process was categorized into three stages. In the first stage, the mixture began to decompose at 130 °C, and the peak temperature of decomposition was 158.3 °C, which indicates that the exothermic reaction between DPT and urea occurred at 130–180 °C. Figure 3(b) shows the reaction formula of DPT combined with urea [24]. The mass loss in the second stage was primarily caused by the decomposition of HMTA and biuret generated in the first stage, which resulted in solid residues. Subsequently, these solid residues decomposed slowly as the temperature increased.

Unreacted active sites remained in the phenolic ring of the structural pre-polymer of the phenolic resin. Therefore, a curing agent must be added to induce a reaction with the active sites on the phenolic ring of the resin molecule such that it can be further solidified into a 3D polymer. It is generally believed that the unreacted active sites in phenolic resin will react with any N atom in HMTA under a small amount of ~5% free phenol and less than 1% water in the system, resulting in an active hydrogen transfer reaction on the active sites of the phenolic ring [27]. The curing reaction process is illustrated in Fig. 3(c). Studies pertaining to curing products indicated that 66%–77% of N atoms in HMTA finally combined into the cured products. Therefore, each HMTA molecule lost one N atom, and only NH_3 was produced during curing without generating water. Curing using HMTA offers the following advantages: First, the curing speed and curing efficiency can be improved; in addition, the material exhibits high stiffness and do not warp easily after being cured [28].

3.2 Characteristics of composites

3.2.1 Infrared spectra of materials before and after foaming

To further investigate and prove the decomposition reaction when DPT and urea are used simultaneously, the four preforms after impregnation with the binder and drying were hot-pressed at 60 and 160 °C, respectively, for 10 min to form a thin sheet with a thickness of 0.75 mm. The infrared spectra of different
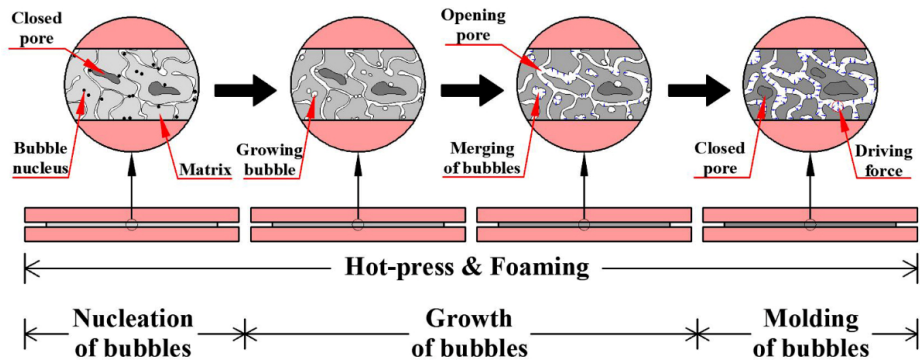
Fig. 3 Decomposition reaction of (a) DPT and (b) mixture of DPT and urea; (c) curing reaction process of phenolic resin by HMTA.

samples that were hot-pressed at 60 and 160 °C are presented in Fig. 4. As shown in Fig. 4(a), the characteristic peaks of DPT and urea did not appear after low-temperature and high-temperature film pressing. This was because the foaming system was not added to F1. By contrast, as presented in Figs. 4(b)–4(d), the characteristic absorption peaks of DPT and urea appeared in the spectra of F2, F3, and F4 after low-temperature film pressing. However, it is noteworthy that the characteristic absorption peaks of

DPT at 1,265 cm^{-1} and urea at 1,622 cm^{-1} of F2, F3, and F4 disappeared after high-temperature film pressing, indicating that both DPT and urea decomposed at 160 °C. The decomposition of DPT and urea can generate a significant amount of gas to form the material, and the reaction between them is shown in Fig. 3(b).

3.2.2 Pore structure

As shown in Fig. 5, the foaming process of paper-

Fig. 4 Infrared spectra of (a) F1, (b) F2, (c) F3, and (d) F4 before and after decomposition of foaming agent.

Fig. 5 Foaming process of paper-based friction materials.

based friction materials can be categorized into three stages: nucleation, growth, and molding of bubbles. First, a blowing agent was added to the molten polymer, and it dispersed freely in the melt. The blowing agent can decompose under the action of heat or a catalyst, thereby generating gas to form a gas–liquid solution. When the gas reaches the saturation limit in the solution and forms a supersaturated solution, it can overflow from the solution and disperse in the liquid polymer. Subsequently, bubble cores are formed and surrounded by a thick liquid. Because the pressure in the bubble is inversely proportional to the radius, the bubble with a smaller radius possesses higher internal

pressure. When two bubbles are in close proximity, gas can diffuse from the small bubble to the large bubble, causing them to merge and form a bubble with a larger radius—This is known as bubble growth. Finally, with further improvement in the curing degree of the matrix, the bubbles are stabilized and solidified.

Figure 6(a) shows the mercury injection curves for different composites. It was discovered that the amount of mercury injected into the material per unit mass increased gradually as the amount of DPT increased; this indicates that F4 had a larger pore volume per unit mass compared with the others. In addition, the slope of the mercury injection curve
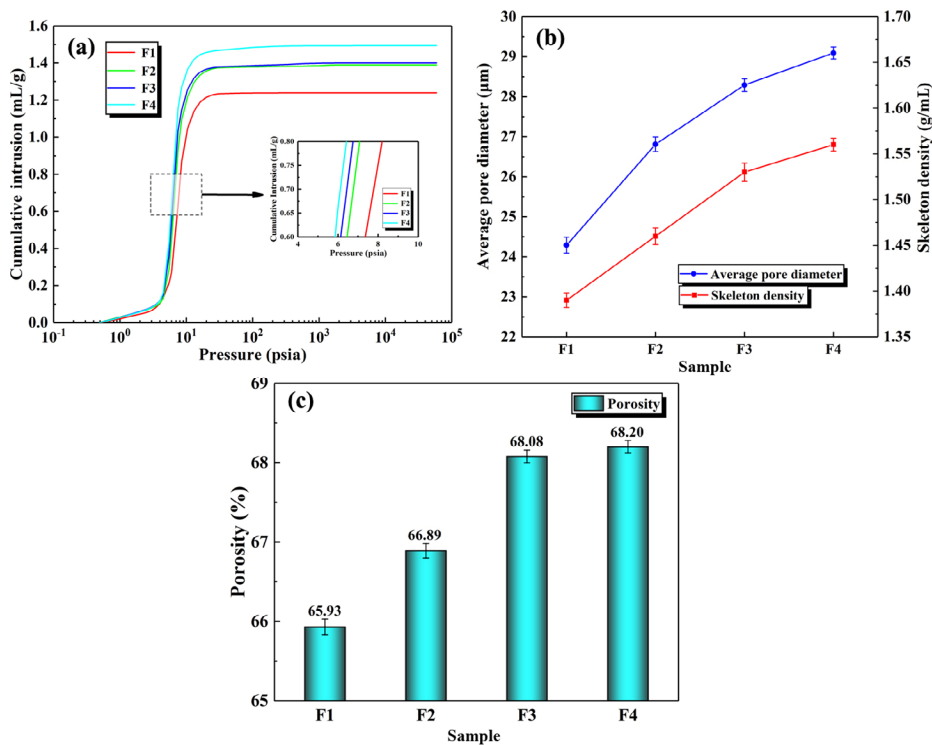

Fig. 6 (a) Mercury injection curves, (b) average pore diameters and skeleton densities, and (c) porosities of F1, F2, F3, and F4.

increased gradually from F1 to F4 in the pressure range of 4–10 psia, which indicates that the efficiency of mercury injection improved gradually and that the penetration of mercury became easier. It can be summarized that the number of opening pores and the connectivity of pores inside the composites increased gradually with the DPT content.

Figure 6(b) shows the average pore size and skeleton density of different materials. As shown in Fig. 6(b), both parameters exhibited a gradually increasing trend. The average pore diameter of F4 was 29.09 μm, which was approximately 19.8% larger than that of F1 (24.29 μm). This is due to the growth of bubbles or the combination of two or more pores during the foaming process, which increased the average pore diameter of the material. As the foaming agent content increased, more bubbles were generated for merging, thereby resulting in larger pore diameters in the material. In addition, the increase in the skeleton density was attributed to the increase in the cross-linking degree of the matrix from a microscopic perspective. The cross-linking of the matrix is a process in which linear polymer chains are connected to form a network polymer via covalent bonds. However, it is noteworthy that not every linear polymer chain participates in the cross-linking reaction. The introduction of the foaming process can provide a driving force for the cross-linking reaction of polymer chains, as shown in Fig. 5, thereby reducing the number of unreacted linear polymer chains and increasing the cross-linking degree of the matrix; consequently, the skeleton density will increase.

Porosity is a critical performance index for wet friction materials and can significantly affect the mechanical and tribological properties of composites. As shown in Fig. 6(c), the porosity of the different materials exhibited a gradual upward trend. The amount of gas generated via thermal decomposition increased significantly as the amount of added DPT increased, and more gas bubbles occupied a larger volume inside the material after the bubbles grew and merged. Subsequently, the bubbles escaped and formed a large number of pores in the material, thereby increasing the porosity of the material.

3.2.3 Surface properties

To investigate the effect of the chemical foaming process on the surface morphology of the composites, the material surface to be rubbed before wear was characterized via SEM, as shown in Fig. 7. It was observed that the fibers, matrix, and fillers were uniformly dispersed, disorderly arranged, and combined. As the DPT content increased, the size and number of pores in the materials increased after the foaming
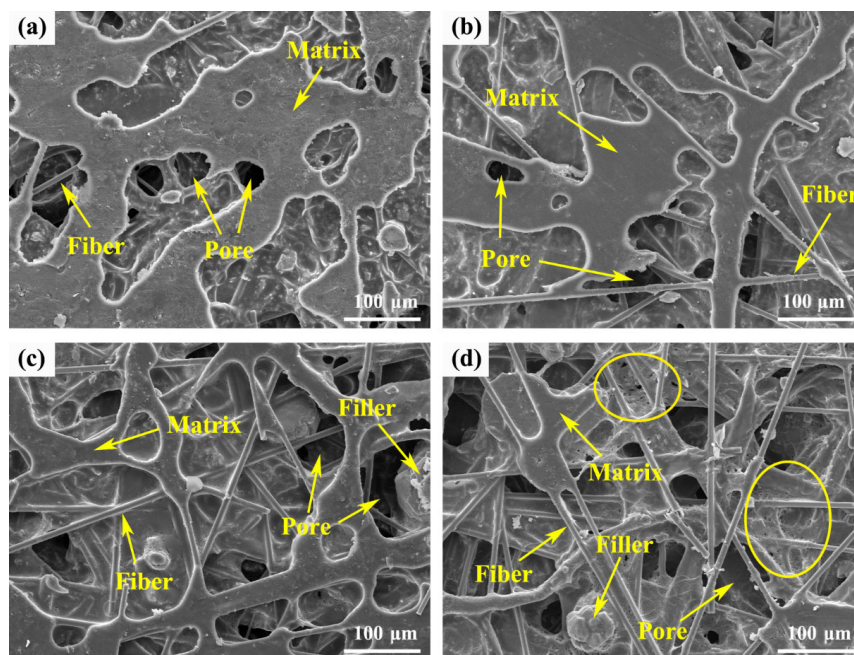

Fig. 7 SEM micrographs of (a) F1, (b) F2, (c) F3, and (d) F4 before wear.

process. As shown in Fig. 7(a), the surface of F1 was shielded with numerous matrices, and only a few fibers were exposed; furthermore, the fillers were wrapped by the matrix. Hence, the synergistic reinforcement effect of each component of the composite could not be fully exerted, stress could not be effectively transferred to the reinforced fibers, and the matrix can peel off easily during the friction process, thereby negatively affecting the wear resistance of the material. As shown in Figs. 7(b)–7(d), the fibers, matrix, and fillers of F2, F3, and F4 were combined well and exhibited larger pore diameters and porosities compared with F1. This shows that the composites that underwent chemical foaming exhibited a better open pore structure, which is conducive to the flow of lubricating oil inside the material. The excellent fluidity of lubricating oil can remove a significant amount of friction heat generated by continuous braking and effectively reduce the thermal wear of materials. In addition, Fig. 7(d) shows that numerous small pores appeared in some areas of the F4 matrix (marked by circles). This might be because when the added amount of DPT was extremely high, the nucleated bubbles did not have sufficient energy to grow; hence, they escaped rapidly from the material when the temperature increased significantly.

Based on the anisotropy of the surface morphology of wet friction materials, the 3D measurement method of all points in the measurement area can be utilized to comprehensively evaluate the characteristics of the surface profile. Figure 8 shows the roughness and
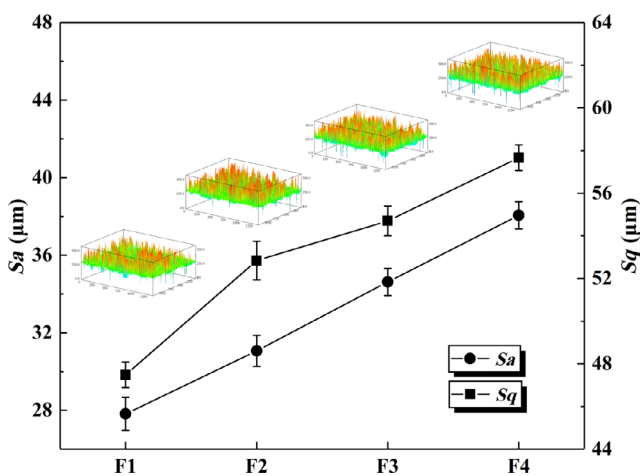

Fig. 8 3D surface profiles and fiction surface roughness of F1, F2, F3, and F4.

3D surface profile of the unworn friction surface of different samples measured using a real color confocal microscope. The surface roughness (Sq) of F1, F2, F3, and F4 was 47.48, 52.84, 54.70, and 57.66 μm, respectively, and Sa indicated a similar tendency. Hence, it can be concluded that both Sa and Sq increased gradually with the increase in DPT, which is consistent with the variations in the average pore size and porosity. As the average pore diameter and porosity increased, the size of the pores and the number of grooves increased, and more fibers and fillers were exposed. All of the above conditions can increase the Sq of the material, based on the calculation principle of Sq [29, 30]. The significant improvement in Sa and Sq implies that the friction surface had a higher Sq value, which is associated closely with the increase in μ_d.

3.2.4 Wettability

Wettability is an important characteristic of wet friction materials and can be affected by two factors. First, it can be affected by the intrinsic properties of the material, depending on whether polar lipophilic groups exist in the molecular structure of the substance. Second, it can be affected by the external properties of the composite, e.g., the surface properties of the solid, such as Sq, porosity, pore diameter, and pore size distribution. To investigate the wettability of lubricating oil on the composites, a set of contact angle experiments were performed, and the results are presented in Fig. 9. As shown in Fig. 9, the contact angles of F1, F2, F3, and F4 were 70.3°, 57.3°, 49.1°, and 37.1°, respectively. The sample indicated better wettability as the amount of DPT added increased, which indicates that the sample possessed better lubricating oil permeability after the chemical foaming process. The improvement in wettability is attributable to the increase in the Sq, porosity, and pore size. Specifically, according to Cassie's theory, the apparent contact angle decreases as the surface roughness increases for a surface with a contact angle less than 90° [31]. In addition, an increase in porosity and pore diameter can result in a decrease in compactness. Consequently, the proportion of solids per unit area on the surface is reduced, resulting in a reduced flow resistance of the lubricating oil to facilitate the spread of oil droplets, as illustrated in Fig. 9(e).
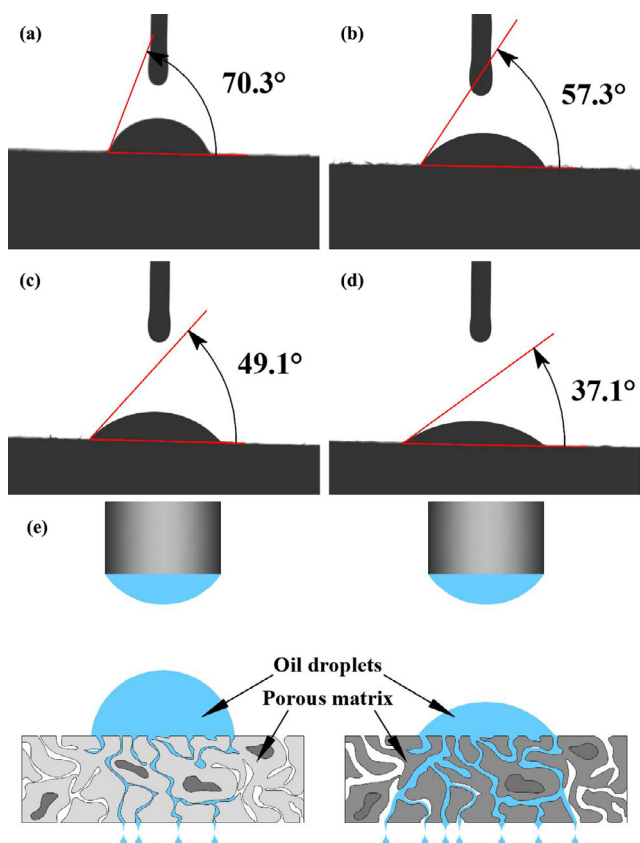
Fig. 9 Contact angles of (a) F1, (b) F2, (c) F3, and (d) F4; (e) schematic diagram of improvement mechanism of wettability.

3.3 Thermal and mechanical performances

3.3.1 Thermal characterization

In the continuous braking process, a significant amount of frictional heat can be generated. If the heat cannot be effectively dissipated or transferred in time, then the surface temperature of the friction materials will increase rapidly, which can in fact damage the materials. To investigate the effect of the chemical foaming process on the paper-based friction materials, the thermal stabilities of the four samples were analyzed using TG-DTG curves. As shown in Fig. 10(a), the temperature at which the mass loss was 10% was 337.8 °C for F1, which was higher than those for F2, F3, and F4. However, F1 exhibited a higher weight loss rate as the temperature increased. The residual mass percentage of the four composites after a TG evaluation was 46.86% for F1, 50.95% for F2, 52.03% for F3, and 53.24% for F4, when the temperature increased to 600 °C. The results show that F4 exhibited better thermal stability compared with the others.

Figure 10(b) shows the DTG curves of the composites. Two primary decomposition peaks were observed, i.e., at 300–350 °C and 500–560 °C, which were primarily attributed to the thermal degradation of nitrile rubber and phenolic resin. Nitrile rubber exhibited two rapid weight loss stages: The first stage occurred within 360–500 °C, and severe thermal decomposition occurred at this time. Furthermore, the molecular chain underwent thermal cracking at this stage, and the degree of chain breaking increased as the pyrolysis reaction progressed. The second stage occurred at temperatures beyond 500 °C, and the main reaction was oxidation, which can produce solid carbon. However, because the heat resistance of nitrile rubber is inferior, the mass loss reached up to 90% when the temperature exceeded 500 °C [32, 33].

The thermal degradation of phenolic resins can be categorized into three stages [34]. The temperature range of the first stage was 100–300 °C. Small molecules such as H_2O, CO_2, and glycol adsorbed into the porous structure of wet friction materials volatilize when heated. The weight loss at this stage was primarily caused by the physical desorption of small molecules with no chemical reaction. Therefore, the difference in the thermal stability of the samples was insignificant. The second stage occurred in the temperature range of 300–360 °C. At this stage, CO_2 molecules, hydroxyl, aromatic rings, and other functional groups were present in the gas products owing to the volatilization of free phenol in the phenolic resin. In addition, a slight condensation reaction of hydroxyl groups, a bond-breaking reaction of methylene groups, and an oxidation reaction involving hydroxyl radicals occurred at this stage, as presented in Fig. 10(c) [35]. Figure 10(c) shows that the phenolic hydroxyl active groups can further undergo condensation polymerization with methylene to generate small molecules of H_2O at approximately 350 °C, which will further increase the cross-linking degree of the resin matrix. As shown in Fig. 10(b), the decomposition peak temperature of F1 was 305.6 °C at this stage, which was lower than those of F2, F3, and F4. This is primarily due to the formation of HMTA after the foaming process; the formed HTMA can react with free phenol, thereby resulting in less free phenol in the phenolic resin. In addition, the squeezing force caused by the growth and
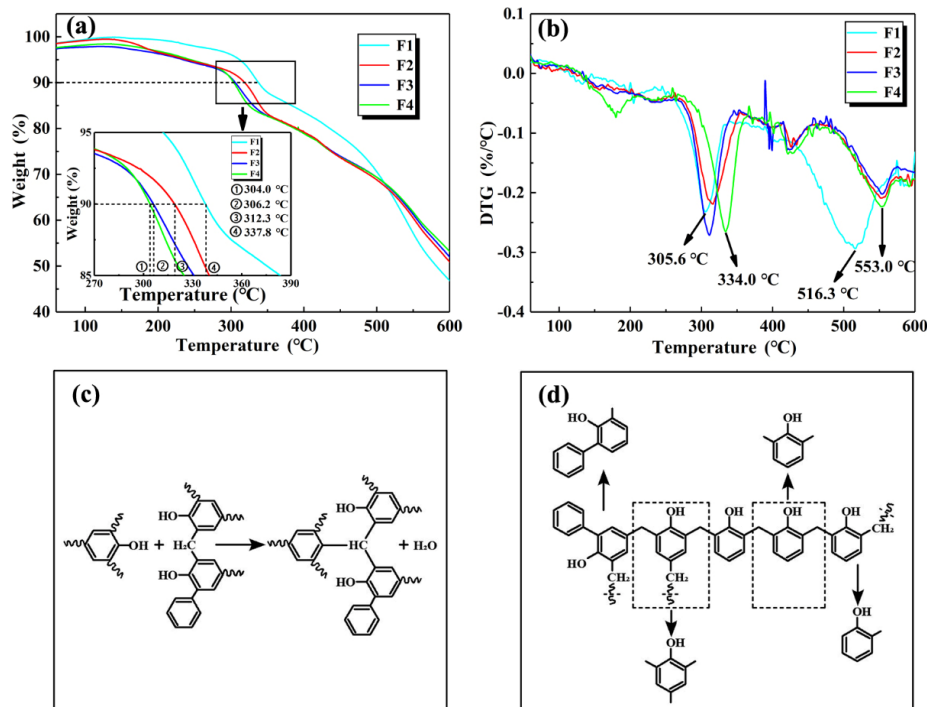
Fig. 10 (a) TG and (b) DTG curves of samples; (c, d) chemical reaction formulae for thermal degradation of phenolic resin.

expansion of bubbles can improve the curing degree of the phenolic resin, thereby increasing the bonding strength between molecules and rendering it more difficult to break the methylene bond. The third stage occurred at 500–650 °C, which was the main decomposition stage of the phenolic resin. With a further increase in temperature, methyl phenol, dimethyl phenol, and O-phenyl phenol appeared in the gas products at 500 °C, which was due to the bond breaking of the methylene groups of the resin molecular chain, as shown in Fig. 10(d) [34]. The weight loss at this stage was caused by the volatility of a significant amount of aromatic gas produced by the molecular chain scission reaction of the phenolic resin. As shown in Fig. 10(b), the decomposition peak temperature of F1 was 516.3 °C at this stage, which was much lower than that of F4 (553.0 °C). This is primarily due to the introduction of the chemical foaming process, which provided a driving force for the curing of the binder, as shown in Fig. 6, and caused a significant increase in the curing efficiency of the samples, thereby enhancing the hardness and modulus of the matrix (Section 3.3.2). This implies that the strength of the methylene chemical bond and the intermolecular bond improved and resulted in a

higher temperature, which is necessary to break the methylene bond. Based on the analysis above, it can be concluded that the introduction of the chemical foaming system can effectively improve the heat resistance of the material, i.e., it can decelerate the thermal degradation of the matrix and reduce the thermal wear of the materials.

3.3.2 Nanoindentation hardness and elastic modulus

The hardness and elastic modulus significantly affect the friction and wear properties of friction materials [36]. Reference [37] shows that increasing the hardness of composite materials results in a lower wear rate. To measure the hardness and elastic modulus of different samples, an indenter was used to perform an indentation test on the matrix of the material under a maximum load of 100 mN, and the results are shown in Fig. 11. As shown in Fig. 11(a), the hardness of F4 was 0.172 GPa, which is an approximately 73.7% increase compared with that of F1 (0.099 GPa). Two factors contributed to the increase in the hardness. First, the formation of decomposition product HMTA can increase the curing efficiency of the phenolic resin such that it can be cured further into a 3D polymer. Second, the growth and expansion of a numerous
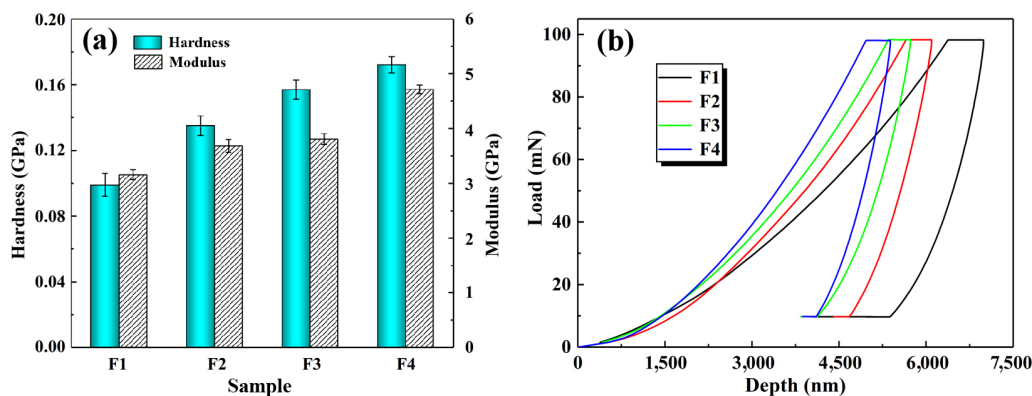
Fig. 11 (a) Hardness and elastic modulus and (b) load–depth curves of F1, F2, F3, and F4.

bubbles can exert a squeezing force on the matrix during the foaming process, which will then increase the cross-linking degree of the matrix. Consequently, the curing degree of the phenolic resin and the vulcanization degree of the nitrile rubber will improve, thereby causing the strength of the materials to enhance significantly. In addition, the elastic modulus of F4 was 4.715 GPa, which was approximately 49.4% higher than that of F1 (3.155 GPa). The elastic modulus can be used as an index to measure the difficulty of elastic deformation of materials; a greater elastic modulus, from a microscopic perspective, implies a greater bonding strength between atoms, ions, or molecules. A material with a greater elastic modulus requires a greater stress to generate a certain elastic deformation, that is, the greater the stiffness of the material. Figure 11(b) shows the load–depth curves of the different samples. As shown in Fig. 11(b), the entire test process primarily comprised three stages: loading, load holding, and unloading stages [38]. The indentation depth directly reflects the hardness of the sample. The lower the indentation depth, the higher is the hardness of the sample [39–41]. As shown in Fig. 11(b), the indentation depth of F4 was the lowest under the maximum load, indicating that F4 possessed the highest hardness. The results confirmed that the introduction of the chemical foaming process can increase the hardness and elastic modulus of the material.

3.3.3 Compressibility and recovery properties

Figure 12 shows the average values of compressibility and recovery of different composites after three cycles under a load of 50 N. The results show that the compressibility of F4 was 5.9%, which was 79% higher than that of F1 (3.3%), and showed an increasing trend. The recovery increased from 83.8% (F1) to 89.0% (F3), and then decreased slightly to 86.6% (F4). The flow of lubricating oil in the pores of materials can remove a significant amount of heat generated during braking. A sample with greater elasticity is conducive to the flow of lubricating oil, thereby reducing the heat loss of the materials [3]. The compressibility is primarily affected by porosity. The higher the porosity, the larger is the load on the pore wall per unit area, which results in a more significant compression deformation. Meanwhile, the material can recover after braking, and a good recovery enables more lubricating oil to be absorbed such that a thicker lubricating oil film can be formed to protect the friction surface during the next braking process. Owing to the synergistic effect of the improvement in the curing degree of the matrix and the modification of nitrile rubber, the
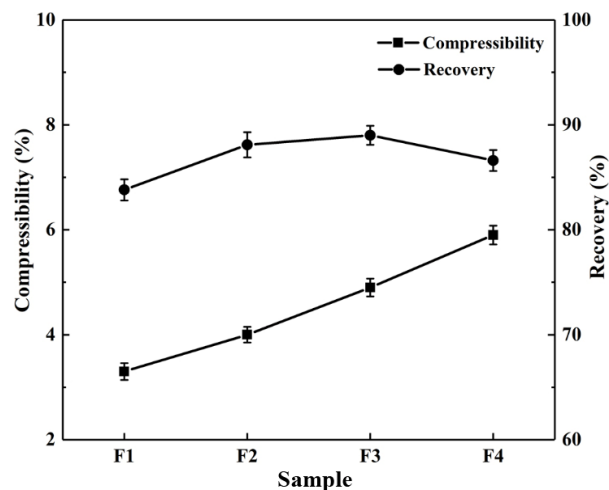

Fig. 12 Compressibility/recovery of different materials.

recovery rate increased gradually. However, because F4 possessed high porosity, the pores with thin pore walls crushed easily and yielded partial permanent deformation, which slightly deteriorated the recovery of the sample. The ideal wet friction material must exhibit high compressibility and recovery such that the material possesses favorable elasticity, which is beneficial for improving friction and wear performance.

3.4 Wet tribological performance

The stability of μ_d is vital to braking materials; it is typically measured by the fluctuation of μ_d during a repeated braking process. The stability of μ_d can directly affect the braking stability and safety of machinery. Figure 13(a) shows the μ_d obtained from 200 times of continuous braking under 0.5 MPa and 2,000 rpm. It can be concluded that F3 and F4 demonstrated better friction coefficient stability than the others; furthermore, it was shown that μ_d decreased slightly in the first 20 braking cycles, and then gradually stabilized. The main factors affecting the friction coefficient stability of paper-based friction materials are the morphology and temperature of the friction interface. The reinforcement fibers on the friction surface of F1 were primarily shielded by the matrix owing to the low porosity, as shown in Fig. 7(a). In the continuous braking process, the matrix is peeled off easily from the material, which renders the rough peaks on the friction surface fluctuate easily, thereby resulting in inferior friction stability. In addition, friction heat can accumulate endlessly during the continuous braking process, and a high friction interface temperature can soften the material,

thereby reducing the strength of the material and deteriorating the friction stability. Because lubricants have better fluidity in composites with larger porosities and pore diameters, they can contribute maximally to the cooling effect of lubricants to enhance the stability of μ_d.

The wet friction materials used in this study are primarily used in wet transmission systems, which require the μ_d to be as high as possible within a certain range. As shown in Fig. 13(b), the average μ_d values of F1, F2, F3, and F4 were 0.1473, 0.1643, 0.1696, and 0.1756, respectively, showing a gradual increasing trend. The improvement in μ_d is attributable to the following factors: First, the introduction of chemical foaming can improve the Sq of the material, which can then increase the degree of engagement between the friction material and friction pair. Therefore, the friction torque that overcomes the mechanical action during the braking process increases, resulting in an improved μ_d. Second, the porosity and average pore diameter of the composites continue to increase as the contents of DPT and urea increase; as such, the fluidity of the lubricant on the surface and inside the material improves. The good fluidity of the lubricating oil can thin out the lubricating oil film during braking, thereby increasing the meshing degree between the micro-protrusions on the friction surface and the friction pair [42]. Consequently, a greater friction force is required to overcome this mechanical engagement, thereby resulting in an increase in the friction coefficient. Additionally, it can remove a significant amount of heat to prevent the reduction in the fixation degree of the Sq peaks by the matrix, thereby resulting in a lower μ_d. In addition, the increase in hardness and
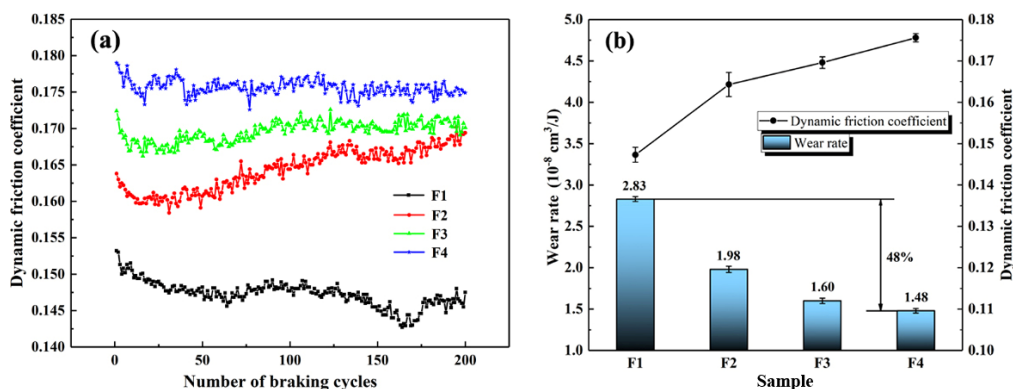

Fig. 13 (a) Dynamic friction coefficients and (b) wear rates of different composites.

elastic modulus indicates an increase in the Sq peak strength; therefore, a larger friction force must be applied during braking, which can increase μ_d. Finally, the number of contact rough peaks can increase under the same braking pressure owing to the increase in compressibility, which results in an increase in μ_d.

Figure 13(b) shows the wear rate of different composites. It can be concluded that the wear rate reduced significantly after foaming treatment. The wear rate of F4 was 1.48×10^{-8} cm^3/J, which was an approximately 47.7% decrease compared with that of F1 (2.83×10^{-8} cm^3/J). The improvement in wear performance was primarily due to the following reasons. As shown in Figs. 7(b)–7(d), the samples after foaming treatment yielded better interfacial bonding, and the fibers, binder, and fillers were evenly distributed and well bonded, thereby allowing each component of the composites to contribute maximally. The excellent interfacial bonding can reduce fiber pullout, matrix peeling, and rough peak fracture, as well as prevent the formation of abrasive particles, thereby improving the wear performance. By contrast, the friction surface of F1 was shielded by the matrix, as shown in Fig. 7(a); as such, the reinforcing effect of the fiber could not be fully exerted. Under a continuous shear stress, the matrix cracked or peeled off easily,

causing an increase in the wear rate. Subsequently, a higher temperature of the friction interface can soften or destroy the material and reduce the strength of the rough peaks. The decrease in the strength of the material causes the material to fracture easily and produce abrasive particles under a continuous sliding friction, thereby aggravating the abrasive wear of the material. The increase in porosity and average pore diameter can accelerate the flow of lubricating oil inside the composites; as such, the composites can contribute maximally in reducing the interface temperature and effectively preventing the strength reduction of the roughness peaks. Finally, the introduction of a chemical foaming process can enhance the curing degree of the binder. Consequently, the hardness and elastic modulus of the matrix will be improved, and hence favorable wear resistance can be achieved.

As shown in Fig. 14, some changes occurred in the surface morphology of the samples after wear. In the continuous braking process, the friction surface was subjected to cyclic contact stresses and deformation, which resulted in the generation and propagation of cracks, as shown in Fig. 14(a). When the braking process continued, debris or particles peeled off from the friction surface, thereby resulting in fatigue wear. Moreover, it was discovered that the worn surface
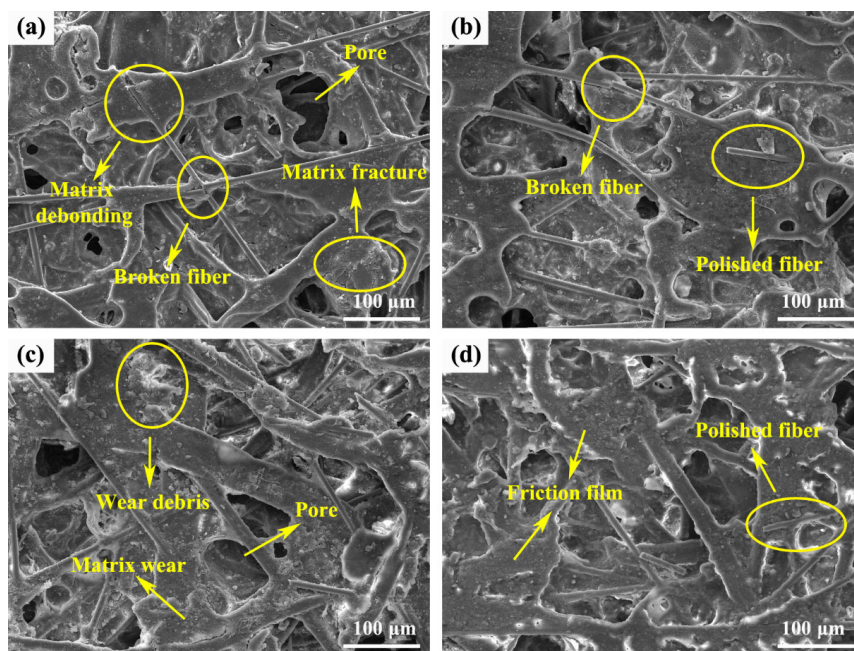

Fig. 14 SEM micrographs of (a) F1, (b) F2, (c) F3, and (d) F4 after wear.

became rougher than the surface before the wear. The wear debris formed by matrix peeling and fiber fracture adhered to the friction surface or filled the pores, causing abrasive wear. The friction surface of F1 showed more fiber debonding and matrix fracture, as presented in Fig. 14(a), owing to the inferior interfacial bonding and matrix strength. By contrast, F4 presented a relatively smoother surface with less damage, as shown in Fig. 14(d), which implied excellent wear resistance.

4   Conclusions

In summary, the introduction of chemical foaming technology to the traditional wet friction material preparation process can effectively change the pore structure of the material, i.e., an increase in the skeleton density, total pore area, average pore diameter, and porosity. After the optimization of the pore structure, the interface bonding, Sq, and wettability of the materials improved significantly, which was conducive to the improvement in the friction and wear properties. Using DPT and urea as the foaming system, the thermal stability and strength of the matrix improved; this was primarily attributed to the improvement in the curing degree of the matrix. The application of chemical foaming technology afforded simultaneous improvements in the friction and wear properties, i.e., μ_d increased by 19.2%, and the wear rate reduced by 47.7%. This effectively solved the contradiction between the increase in porosity and wear rate. This study provides insights into the modification of the pore structure of paper-based friction materials using chemical foaming technology, as well as provides new ideas for the regulation and optimization of the pore structure of the materials.

Acknowledgements

References

[1] Ompusunggu A P, Sas P, van Brussel H. Distinguishing the effects of adhesive wear and thermal degradation on the tribological characteristics of paper-based friction materials under dry environment: A theoretical study. *Tribol Int* **84**: 9–21 (2015)

[2] Fei J, Wang H K, Huang J F, Zeng X R, Luo W. Effects of carbon fiber length on the tribological properties of paper-based friction materials. *Tribol Int* **72**: 179–186 (2014)

[3] Zhang X, Li K Z, Li H J, Fu Y W, Fei J. Tribological and mechanical properties of glass fiber reinforced paper-based composite friction material. *Tribol Int* **69**: 156–167 (2014)

[4] Fu Y W, Zhou L, Yin T, Luo Z Y, Li H J, Qi L H. A new kind of resin-based wet friction material: Non-woven fabrics with isotropic fiber networks as preforms. *Friction* **9**(1): 92–103 (2021)

[5] Lu J H, Li Y F, Wang Y, Fu Y W. Effect of pre-impregnated organosilicon layer on friction and wear properties of paper-based friction materials. *Wear* **416–417**: 6–13 (2018)

[6] Deng H J, Li X Q, Li M. Influence of porosity of paper-based friction materials on compressure-resilience and tribology properties. *Tribol* **27**(6): 544–549 (2007)

[7] Li H J, Fei J, Qi L H, Fu Y W, Li X T, Wang P Y. Effect of porosity percentage on the friction and wear performance of carbon fiber reinforced paper-based friction materials. *J Inorg Mater* **22**(6): 1159–1164 (2007)

[8] Matsumoto T. Influence of paper based friction material porosity on the practical performance of a wet clutch. *J Jap Soc Tribologis* **41**(10): 816–821 (1996)

[9] Fei J, Luo D, Zhang C, Li H, Cui Y, Huang J. Friction and wear behavior of SiC particles deposited onto paper-based friction material via electrophoretic deposition. *Tribol Int* **119**: 230–238 (2018)

[10] Wang B B, Fu Q G, Liu Y, Yin T, Fu Y W. The synergy effect in tribological performance of paper-based composites by MWCNT and GNPs. *Tribol Int* **123**: 200–208 (2018)

[11] Li C, Fu Y W, Wang B B, Zhang W H, Bai Y H, Zhang L L, Qi L H. Effect of pore structure on mechanical and tribological properties of paper-based friction materials. *Tribol Int* **148**: 106307 (2020)

[12] Matsumoto T. The influence of paper-based friction material porosity on the performance of a wet clutch. *SAE Technical Papers*, 941032 (1994)

[13] Ren Y, Li H, Li K. Influence of curing pressure on the friction performance of a kind of paper based friction material. (in Chinese). *Acta Mater Compos Sin* **24**(4): 118–122 (2007)

[14] Zhu W T, Wang X F, Jiang J, Fu Y W. Effect of porosity percentage on friction and wear performance of resin-based friction materials. (in Chinese). *Lubr Eng* **41**(6): 59–64 (2016)

[15] Cho S H, Kim H K, Sohn J S, Ryu Y, Cha S W. Effect of foaming processes on the reduction of warpage in glass fiber reinforced plastic composites. *J Mech Sci Technol* **33**(9): 4227–4232 (2019)

[16] Zimmermann M V, da Silva M P, Zattera A J, Santana R M. Poly(lactic acid) foams reinforced with cellulose micro and nanofibers and foamed by chemical blowing agents. *J Cell Plast* **54**(3): 577–596 (2018)

[17] Luo Y, Zhang J L, Qi R R, Lu J Q, Hu X L, Jiang P K. Polylactide foams prepared by a traditional chemical compression-molding method. *J Appl Polym Sci* **130**(1): 330–337 (2013)

[18] Li G, Qi R R, Lu J Q, Hu X L, Luo Y, Jiang P K. Rheological properties and foam preparation of biodegradable poly(butylene succinate). *J Appl Polym Sci* **127**(5): 3586–3594 (2013)

[19] Laukaitis A, Žurauskas R, Kerien J. The effect of foam polystyrene granules on cement composite properties. *Cem Concr Compos* **27**(1): 41–47 (2005)

[20] Zirkel L, Münstedt H. Influence of different process and material parameters on chemical foaming of fluorinated ethylene propylene copolymers. *Polym Eng Sci* **47**(11): 1740–1749 (2007)

[21] Ji Y B, Luo H, Shi M, Yang Z, Gong W, Tan H. Study of the rheology and foaming processes of poly(vinyl chloride) plastisols with different foaming agents. *J Polym Eng* **39**(2): 117–123 (2019)

[22] GB/T 13826-2008 Wet type (non-metallic) friction materials. China Quality and Standards Publishing & Media Co., Ltd., 2008.

[23] Fei J, Li H J, Fu Y W, Qi L H, Zhang Y L. Effect of phenolic resin content on performance of carbon fiber reinforced paper-based friction material. *Wear* **269**(7–8): 534–540 (2010)

[24] Zweifel H, Schiller M, Maier R. *Plastics Additives Handbook*. 6th edn. Munich (Germany): Hanser Gardner, 2009.

[25] Liu Y J, Zhu J F, Zhao Y Z. The effect of foaming system and vulcanizing system on the properties of NBR sponge. (in Chinese). *Rubber Ind* **52**(11): 660–663 (2005)

[26] Rowland D G. Practical chemical blowing agents for expanding rubber. *Rubber Chem Technol* **66**(3): 463–475 (1993)

[27] Huang F R, Jiao Y S. *Phenolic Resin and Its Application*. Beijing (China): Chemical Industry Press, 2003.

[28] Zhang C. Study on curing kinetics of phenolic resin. M.S. Thesis. Wuhan (China): Wuhan University of Technology, 2010.

[29] Dong W P, Sullivan P J, Stout K J. Comprehensive study of parameters for characterising three-dimensional surface topography: IV for characterising spatial and hybrid properties. *Wear* **178**(1–2): 45–60 (1994)

[30] Zhou P, Zhao F L. 3D evaluation method of cutting surface topography of carbon/phenolic (C/Ph) composite. *J Wuhan Univ Technol Mater Sci Ed* **26**(3): 459–463 (2011)

[31] Cassie A B D. Contact angles. *Discuss Faraday Soc* **3**: 11–16 (1948)

[32] Fei J, Luo W, Li H J, Huang J F, Ouyang H B, Wang H K. Effects of NBR particle size on performance of carbon fiber-reinforced paper-based friction material. *Tribol Trans* **58**(6): 1012–1020 (2015)

[33] Liu, L, Wang, B X, Qu, Y T, Zhang, B G, Yang, H. Factors influencing thermal degradation of NBR. (in Chinese). *China Rubber Ind* **60**(4): 211–215 (2013)

[34] Liu, Y Z, Shi, J J, Wang, W, Feng, Z H, Yang, Y H. Pyrolysis mechanism of PICA phenolics. (in Chinese). *Aerosp Mater Technol* **46**(6): 68–73, 78 (2016)

[35] Trick K A, Saliba T E. Mechanisms of the pyrolysis of phenolic resin in a carbon/phenolic composite. *Carbon* **33**(11): 1509–1515 (1995)

[36] Liu H J, Liu H L, Zhu C C, Wei P T, Tang J Y. Tribological behavior of coated spur gear pairs with tooth surface roughness. *Friction* **7**(2): 117–128 (2019)

[37] Trevisiol C, Jourani A, Bouvier S. Effect of hardness, microstructure, normal load and abrasive size on friction and on wear behaviour of 35NCD16 steel. *Wear* **388–389**: 101–111 (2017)

[38] Wang B B, Fu Q G, Li H J, Qi L H, Lu Y Y. Synergistic effect of surface modification of carbon fabrics and multiwall carbon nanotube incorporation for improving tribological

properties of carbon fabrics/resin composites. *Polym Compos* **41**(1): 102–111 (2020)

[39] Xia M L, Liu P, Sun Q P. Grain size dependence of Young's modulus and hardness for nanocrystalline NiTi shape memory alloy. *Mater Lett* **211**: 352–355 (2018)

[40] Ma Y, Peng G J, Chen H, Jiang W F, Zhang T H. On the nanoindentation hardness of Cu–Zr–Al/Cu nanolaminates. *J Non Cryst Solids* **482**: 208–212 (2018)

[40] Ma Y, Peng G J, Chen H, Jiang W F, Zhang T H. On the

nanoindentation hardness of Cu–Zr–Al/Cu nanolaminates. *J Non Cryst Solids* **482**: 208–212 (2018)

[41] Li W, Liu J, Zhou Y, Wen S F, Tan J W, Li S, Wei Q S, Yan C Z, Shi Y S. Texture evolution, phase transformation mechanism and nanohardness of selective laser melted Ti-45Al-2Cr-5Nb alloy during multi-step heat treatment process. *Intermetallics* **85**: 130–138 (2017)

[42] Liang H, Guo D, Luo J B. Film forming behavior in thin film lubrication at high speeds. *Friction* **6**(2): 156–163 (2018)

Chang LI. He received his M.S. degree in material science in 2021 from Northwestern Polytechnical University, Xi'an, China. After then, he is now a Ph.D. student in the School of Materials of Northwestern Polytechnical University, Xi'an, China. His research interest is fiber reinforced resin-based friction materials.

Jie FEI. He received his Ph.D. degree in 2009 from Northwestern Polytechnical University, Xi'an, China. He is now working as a full professor at Northwestern Polytechnical University, Xi'an, China. His research interests are carbon fiber reinforced resin-based friction materials and carbon-based composites.

Enzhi ZHOU. He received his B.S. degree in mechanical engineering from Tiangong University, Tianjin, China. He is studying for a M.S. degree at Northwestern Polytechnical University, Xi'an, China. His research focuses on high-performance paper-based friction materials, new fabric-reinforced resin-based friction materials, and friction and wear mechanisms of composite materials.

Rui LU. She received her M.S. degree in 2021 from Northwestern Polytechnical University, Xi'an, China. Her research mainly focuses on the friction and wear properties between friction materials and alumina dual under wet braking condition. She is now working as a quality engineer in a semiconductor company.

Xiaohang CAI. He received his B.S. degree in 2015 from Harbin Engineering University, Harbin, China. He is studying for a M.S. degree at Northwestern Polytechnical University, Xi'an, China. His research focuses on carbon fiber reinforced resin-based friction materials and tribological properties wear mechanism at low temperatures.

Yewei FU. He received his Ph.D. degree in materials science in 2005 from Northwestern Polytechnical University, Xi'an, China. He has overcome many key technologies in the research of advanced preparation technology for high-performance paper-based friction materials.

Hejun LI. He received his Ph.D. degree in plastic processing from Harbin Institute of Technology in 1991. After that, he joined the School of Materials at Northwestern Poly-technical University. From 2002 to 2016, he served as the dean of Materials College of Northwestern Polytechnical University. In 2019, he was elected as the Member of the Chinese Academy of Engineering and the Asia Pacific Academy of Materials. His research interests are advanced carbon/carbon composites, paper-based friction materials, and nanomaterials.